Structure *14*, 1039–1048, June 2006 ©2006 Elsevier Ltd All rights reserved DOI 10.1016/j.str.2006.03.018

Structure of the Bacteriophage ϕ6 Nucleocapsid Suggests a Mechanism for Sequential RNA Packaging

Juha T. Huiskonen,[1] Felix de Haas,[2,3] Doryen Bubeck,[2,4] Dennis H. Bamford,[1] Stephen D. Fuller,[2,4] and Sarah J. Butcher[1,*]

[1] Institute of Biotechnology and
Department of Biological and Environmental Sciences
University of Helsinki
P.O. Box 65 (Viikinkaari 1)
FIN-00014 Helsinki
Finland

[2] Structural Biology Programme
European Molecular Biology Laboratory
Meyerhofstraße 1
69117 Heidelberg
Germany

Summary

Bacteriophage ϕ6 is an enveloped dsRNA virus with a segmented genome. ϕ6 specifically packages one copy of each of its three genome segments into a preassembled polymerase complex. This leads to expansion of the polymerase complex, minus and plus strand RNA synthesis, and assembly of the nucleocapsid. The ϕ6 in vitro assembly and packaging system is a valuable model for dsRNA virus replication. The structure of the nucleocapsid at 7.5 Å resolution presented here reveals the secondary structure of the two major capsid proteins. Asymmetric P1 dimers organize as an inner *T* = 1 shell, and P8 trimers organize as an outer *T* = 13 laevo shell. The organization of the P1 molecules in the unexpanded and expanded polymerase complex suggests that the expansion is accomplished by rigid body movements of the P1 monomers. This leads to exposure of new potential RNA binding surfaces to control the sequential packaging of the genome segments.

Introduction

Bacteriophage ϕ6 is the type member of the *Cystoviridae* family and shares many structural and functional similarities with dsRNA viruses belonging to the *Reoviridae* family. Members of the *Reoviridae* family infect plants, insects, and animals (Mertens, 2004). ϕ6 is a spherical, enveloped virus infecting gram-negative *Pseudomonas syringae* cells. The ϕ6 virion is a triple-layered structure enclosing a segmented dsRNA genome. The outermost layer consists of a lipid membrane with virally encoded integral membrane proteins, P6, P9, P10, and P13 (Gottlieb et al., 1988; Sinclair et al., 1975; van Etten et al., 1976). P6 anchors the receptor binding spike protein P3 to the membrane (Stitt and Mindich, 1983). The membrane surrounds a nucleocapsid (NC) particle with two concentric protein shells. The outer protein shell with a *T* = 13 (*T* for triangulation number [Caspar and Klug, 1962]) icosahedral lattice mainly consists of protein P8 (Butcher et al., 1997) and is denoted here as the NC shell. The main component of the inner protein shell is protein P1 (Butcher et al., 1997). P1, together with proteins P2, P4, and P7, forms the polymerase complex (PC). Here, we denote the inner shell as the PC shell. P2 is the RNA-dependent RNA polymerase located at a radius consistent with its proposed location under the 5-fold vertices (Ikonen et al., 2003; Makeyev and Bamford, 2000). Hexamers of the packaging NTPase P4 form the turrets at the vertices (de Haas et al., 1999). P7 is a packaging factor (Juuti and Bamford, 1995, 1997) and is also suggested to aid in particle assembly (Poranen et al., 2001).

During the viral life cycle, ϕ6 attaches to the host pilus by using the receptor binding spikes formed by protein P3 (Kenney et al., 1992; Romantschuk and Bamford, 1985). The pilus retracts, bringing the viral membrane into contact with the host cell. The membrane bound, spike-anchoring protein P6 then mediates fusion with the host cell outer membrane (Bamford et al., 1987), releasing the NC into the periplasmic space. The viral lytic enzyme (P5) on the NC surface digests the peptidoglycan layer of the host, allowing the NC to enter the cytoplasm via an endocytic-like route (Poranen et al., 1999; Romantschuk et al., 1988). A transcriptionally active PC particle is then released into the host cell cytoplasm, where transcription of the three dsRNA segments (S, M, and L) occurs. The L segment messenger mRNA encodes for five proteins: P1, P2, P4, P7, and P14. The first four assemble into PCs in the cytoplasm. PCs package one of each of the positive sense, single-stranded, viral RNA segments before replicating them into dsRNA and transcribing new mRNAs within the particle. A shell of protein P8 coats the dsRNA-containing PC particles to form the NC. The NC is enveloped in the cytoplasm, and mature virions exit from the host cell by cell lysis. The development of an in vitro ϕ6 NC assembly system (Olkkonen et al., 1990) that uses purified components (Poranen et al., 2001) has allowed a detailed biochemical description of PC assembly, packaging, and replication (Poranen and Tuma, 2004).

A model has been put forward to explain the genome packaging process (Mindich, 2004). The packaging NTPase P4 translocates the three ssRNA segments (s, m, and l) into the PC in a controlled, sequential fashion. The recognition of the segments is based on unique *pac* sequences (200 nt) located at the 5′ end of each segment. First, the PC recognizes and packages the s segment. This packaging reaction is suggested to induce a conformational change inactivating the recognition site for s and creating a recognition site for the m segment, which is followed by the packaging of m. Another change in the particle conformation occurs, leading to the disappearance of the recognition site for m and the creation of a recognition site for the l segment.

*Correspondence: sarah.butcher@helsinki.fi

[3] Present address: PHILIPS/FEI Electron Optics BV, Achteseweg Noord 5, P.O. Box 218, 5600 MD Eindhoven, The Netherlands.

[4] Present address: Oxford Particle Imaging Centre, Division of Structural Biology, University of Oxford, Roosevelt Drive, Oxford OX3 7BN, United Kingdom.

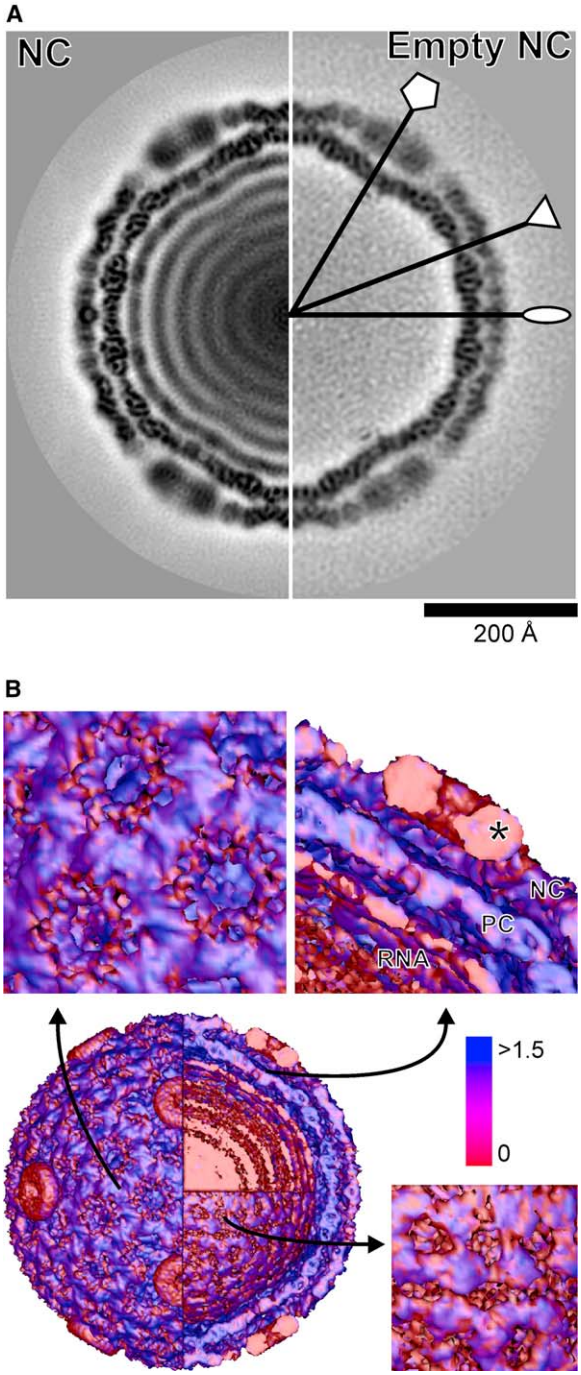

Figure 1. ϕ6 Reconstructions

(A) Halves of the central sections of the reconstructions for the NC (left) and empty NC (right) are shown. Individual icosahedral 2-fold (ellipse), 3-fold (triangle), and 5-fold (pentagon) axes of symmetry are shown for the empty NC. Protein density is black. The scale bar represents 200 Å.

(B) A gradient coloring (see Experimental Procedures) of the isosurface representation of the NC (rendered at 1.2σ above the mean density) to visualize order (blue) and disorder (red). Parts of the NC were removed to reveal inner layers of dsRNA. The arrows indicate the positions of the close-ups. The first close-up (upper row, left) reveals the holes in the outer NC protein shell. In the second close-up (upper row, right), the dsRNA genome (RNA) and the PC and NC shells are indicated. A disordered P4 hexamer is indicated with an asterisk. The third close-up (bottom row, right) reveals the outermost layer of RNA, which is organized in patches and is more ordered than the inner layers. The color bar represents the values of the gradient as standard deviations.

Table 1. Statistics of ϕ6 Reconstructions

	NC	Empty NC
Number of particles	10,463	1,163
Number of micrographs	52	37
Nominal sampling (Å pixel^{-1})	1.4	2.8
Micrograph underfocus range (μm)	0.4–2.5	0.5–2.5
Maximum resolution (Å)[a]	6.0	8.3
Effective resolution (Å)[b]	7.5	12

[a] The resolution to which the maps were calculated.
[b] An estimate for the resolution based on the FSC 0.5 criterion.

Packaging of I switches the particle to minus strand synthesis. As a result of the entire process, the empty dodecahedral PC particle expands into a spherical, dsRNA-containing particle. However, the conformational changes occurring during this process in the inner P1 protein shell are unknown, because, in the previous ϕ6 reconstructions, the organization of the P1 monomers was ambiguous due to the limited resolution (Butcher et al., 1997; de Haas et al., 1999). Based on protein mass measurements (Day and Mindich, 1980), it has been proposed that the inner shell is composed of 60 asymmetric P1 dimers (Butcher et al., 1997). This organization has been observed in eukaryotic dsRNA viruses, such as members of the *Reoviridae* family and the L-A virus (Grimes et al., 1998; Naitow et al., 2002; Nakagawa et al., 2003; Reinisch et al., 2000; Zhou et al., 2003).

In this study, we have determined the structure of the ϕ6 NC by using cryo-electron microscopy (cryo-EM) and three-dimensional (3D) image reconstruction. At 7.5 Å resolution, the folds of the major capsid proteins and the interactions between different structural components are resolved. The structure reveals the extent of similarities between ϕ6 and eukaryotic dsRNA viruses. Based on the PC architecture, we propose a model defining the movement of the P1 subunits during expansion. From the model, it is evident that potential RNA binding sites on the PC shell change dramatically during expansion, and we propose that these changes control the selectivity of packaging. Finally, we suggest that this ϕ6 expansion model also serves as a paradigm for dsRNA viruses infecting eukaryotic hosts.

Results

Order and Disorder in the Nucleocapsid Reconstruction at 7.5 Å Resolution

Purified ϕ6 NCs, which lack the membrane, were subjected to cryo-EM and 3D image reconstruction (Figure 1; Table 1). In the electron micrographs, the NCs appear similar to those described previously (Butcher et al., 1997; Kenney et al., 1992). A data set of 10,463 particle images was used to calculate a 3D reconstruction of the NC (Figure 1A, NC). The resolution was 7.5 Å, judged by using the Fourier shell correlation 0.5 criterion (Harauz and van Heel, 1986). The NC is a multilayered structure (diameter of 595 Å) with outer protein shells

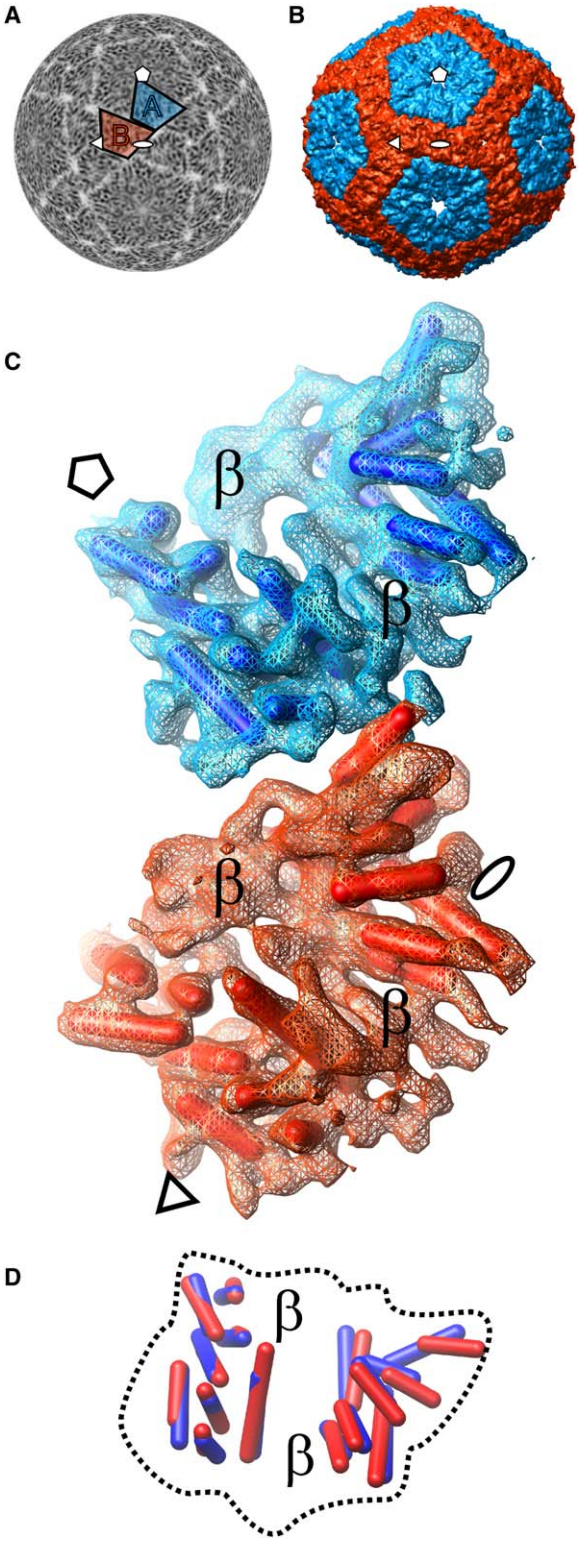

Figure 2. The Inner *T* = 1 Protein Layer

(A) Density layer (at a radius of 228 Å) through the NC reconstruction. The two monomers are labeled with blue (monomer A) and red (monomer B).

(B) Isosurface rendering of the P1 layer at the threshold corresponding to the calculated protein mass (1.2σ above the mean density).

(C) A close-up of the asymmetric protein P1 dimer rendered at a higher threshold (2.6σ) to reveal the inner details. The putative α helices are shown as 5 Å thick rods, and the β sheet-containing regions are marked with "β." The color coding for monomers A and B in (B) and (C) is as in (A). The symmetry axes in (A)–(C) are labeled as in Figure 1A.

(D) The putative α helices for monomers A (blue) and B (red) are superimposed to reveal the similarity in their organization.

enclosing the RNA genome. To identify the RNA component of the virus, we calculated a reconstruction by using images of NCs, which had spontaneously lost the genome (Figure 1A, Empty NC; Table 1). This reconstruction defined the two outermost layers as protein (radii of ~205–295 Å) and the inner density as RNA. The RNA is organized into six concentric layers (Figure 1A, NC). The average center-to-center spacing between the layers is 31 Å.

The regions containing the genome, the polymerase, and the hexamers of packaging NTPase P4 are expected to be disordered in the icosahedrally averaged reconstruction, as they deviate from icosahedral symmetry: the genome consists of three linear, unique RNA segments, the polymerase is only present in a few copies (Day and Mindich, 1980), and the P4 hexamers are located on the icosahedral 5-fold symmetry axes (de Haas et al., 1999). To accurately localize disorder, and thus to analyze regions of symmetry mismatch, we developed a gradient visualization method (see Experimental Procedures). The steeper the density gradient is at any given position, the better defined the molecular surface. For visualization, we map the value of the gradient, by using a color scale, on the isosurface representation of the density. The method revealed that in the NC reconstruction, the two protein layers are highly ordered (Figure 1B). Major exceptions are evident around the holes in the NC shell and at the position occupied by the P4 hexamer. The RNA genome appears to be less ordered than the protein shells. The outermost layer of RNA is ordered in patches, possibly through interactions with P1, whereas the inner layers appear to be less ordered.

The Polymerase Complex Shell Is Composed of Asymmetric P1 Dimers Organized on a *T* = 1 Lattice

The PC shell is slightly convex at the vertices, with a smaller vertex-to-vertex distance (455 Å) than facet-to-facet (485 Å) and edge-to-edge (480 Å) distances. Volume segmentation of the ϕ6 PC shell revealed a *T* = 1 triangulation (Figures 2A and 2B). One asymmetric P1 dimer of monomers A and B is present in the asymmetric unit (Figure 2A), and thus the copy number of the protein is 120, as proposed previously (Butcher et al., 1997). Class A monomers encircle the 5-fold axes, while class B monomers form a dodecahedral skeleton (Figures 2A and 2B). The two monomers are remarkably similar (Figure 2C). The density assigned to P1 accounts for 80% of the PC shell density between radii of 205–250 Å. The unassigned densities, present mainly at the 3-fold and 5-fold axes (see Figure 5B), may have contributions from any of the four capsid proteins. There was no density that specifically matched the polymerase structure (Butcher et al., 2001), in contrast to reovirus at this resolution (Zhang et al., 2003).

At 7.5 Å resolution, we could analyze the P1 (85.0 kDa) fold, or, more precisely, the spatial relationship between its secondary structure elements. Based on the secondary structure prediction (Cuff and Barton, 2000)

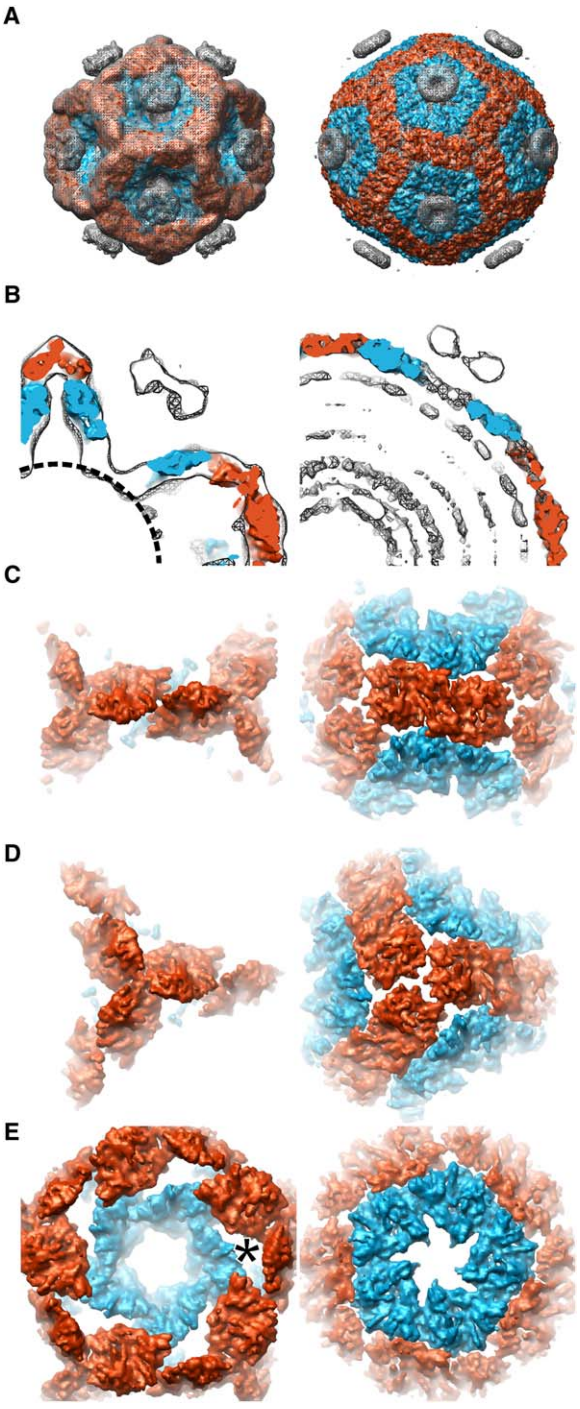

Figure 3. Model for Polymerase Complex Expansion

(A) The change in conformation from the unexpanded (left) (de Haas et al., 1999) to the expanded (right) PC was modeled by treating the segmented P1 monomers (blue and red) as rigid bodies.

(B) A partial slice through the center of the maps. The ring-shaped satellite densities in (A) and (B) correspond to the P4 hexamer and are connected to the P1 shell at a lower threshold (see also Figure 5B). The radius at which the polymerase P2 was localized previously (110 Å) (Ikonen et al., 2003) is indicated with a dashed line on the unexpanded PC. The mesh surface for the unexpanded PC reconstruction was rendered at 1σ, and that for the core model was rendered at 2σ, above the mean density in (A) and (B).

(C–E) Close-ups of the 2-fold, 3-fold, and 5-fold views are shown in (C), (D), and (E), respectively. The large holes between the A and B monomers in the unexpanded form (one marked with asterisk in [E]) are also present in the reconstruction when rendered at a high threshold (not shown). The surfaces for the P1 monomers were rendered at 2σ.

(Figure S1; see the Supplemental Data available with this article online), P1 is a mixed α/β protein with 23 α helices (Figure S1; α1–α23; 5–32 residues, median length is 11 residues) and three separate β strand-rich regions (Figure S1; β1–β5, β11–β15, and β20–β23). From the 3D reconstruction, we computationally identified (Jiang et al., 2001) 15 putative helices (5–21 residues, median length is 11 residues). Two helices in the density probably account for the one long predicted α helix (Figure S1; α6, 32 residues). The helices are clustered into two sets, separated by two visually identified β sheet regions (Figure 2C). The comparison of the arrangement of the helices between A and B monomers reveals the primary differences mainly at the A-B interfaces (Figure 2D). Conformational variability is needed to accommodate for different interactions between the two monomers (Grimes et al., 1998).

Model for the Polymerase Complex Expansion

The expansion of the PC results in a ~2.4-fold difference in the interior volume. The interior volume of the unexpanded PC is $\sim 17.4 \times 10^6$ Å^3, in contrast to $\sim 42.4 \times 10^6$ Å^3 in the expanded PC. The protein composition of the particle remains the same during the expansion. To explain this dramatic conformational change, we modeled the relative translations and rotations of the P1 subunits (Figure 3; Movie S1). This model used the previous 25 Å resolution reconstruction of the unexpanded PC (de Haas et al., 1999) and the PC shell structure described here (Figure 2B). We manually fitted the segmented P1 monomers (Figure 2C) into the unexpanded structure (Figures 3A and 3B, left). For comparison, an NC-P8 difference map with P4 proteins (see below) served as a model for the expanded PC (Figures 3A and 3B, right).

Rigid body rotations of the P1 monomers (35° for monomer A, 46° for monomer B) largely explain the expansion. Local conformational changes at the P1 monomer-monomer interfaces are expected to occur in different expansion states because the angles between different components change dramatically. For example, the class B P1 monomers rotate relative to each other from an angled conformation to a nearly flat conformation at the 2-fold (Figure 3C) and 3-fold (Figure 3D) axes. At the 5-fold axes, the expansion changes the angle between the class A monomers even more, and it also reduces the buried surface area (Figure 3E). In addition, the relative positions of P1 and P4 change. In the unexpanded form, the sides of the P4 hexamer are proximal with the surrounding P1 layer (Figure 3E, left). In the expanded form, however, the base of the hexamer is closest to the underlying P1 layer (Figure 3B, right).

The Nucleocapsid Shell Is Composed of P8 Trimers Organized on an Incomplete *T* = 13 Laevo Lattice

The next step in the assembly pathway after PC maturation is the incorporation of protein P8 on top of the PC, resulting in the NC. The NC shell has a spherical shape, as illustrated by similar facet-to-facet (545 Å)

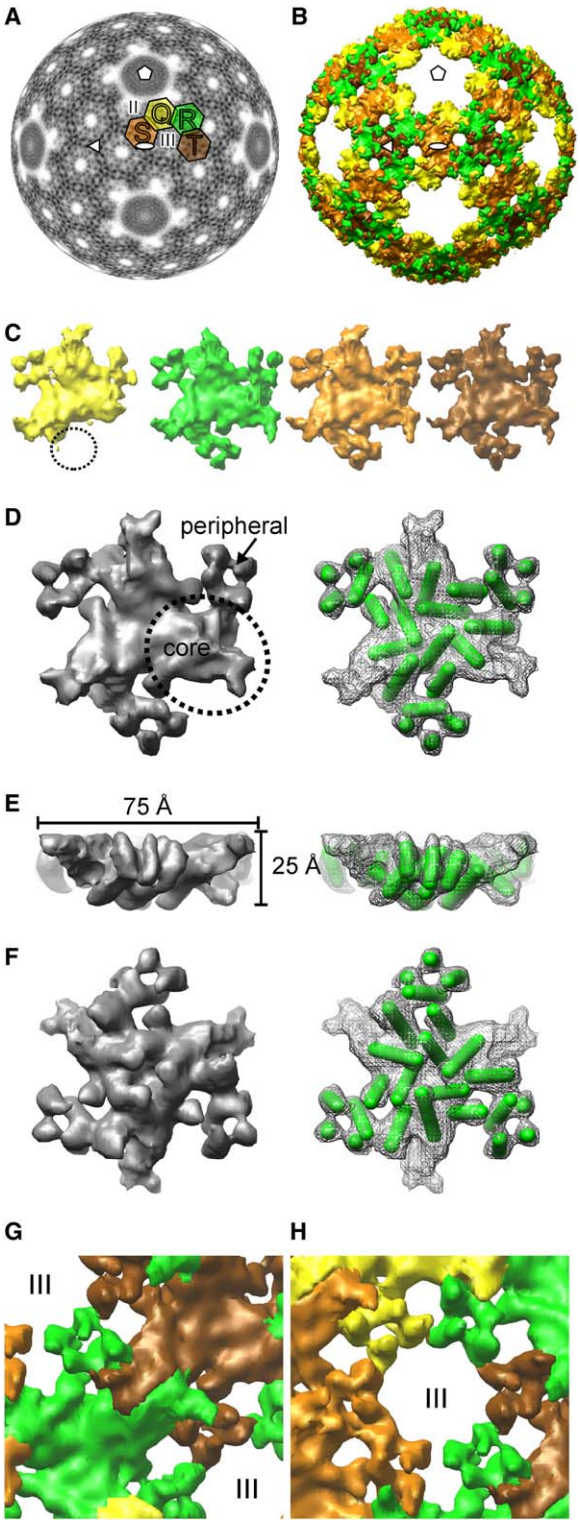

Figure 4. The Outer T = 13 Protein Layer

(A) Density layer (at a radius of 263 Å) through the NC reconstruction. The four unique P8 trimers are labeled with Q (yellow), R (green), S (light brown), and T (brown).

(B) Isosurface rendering of the P8 layer at the threshold corresponding to the calculated protein mass (1.2σ above the mean density). The symmetry axes in (A) and (B) are labeled as in Figure 1A.

(C) A line-up of the individual unique P8 trimers. A disordered part observed in trimer Q (yellow) is circled.

(D–F) The averaged P8 trimer rendered as a solid isosurface (left) and as a mesh surface (right) is seen from the (D) top, (E) side, and (F) bottom. The putative α helices are shown as 5 Å thick rods.

(G–H) Capsomer-capsomer interactions between the core domains at the (G) (quasi) 2-fold positions and (H) between the four-helix bundle domains around the holes at quasi 6-fold positions. The holes (II and III) are denoted in (A), (G), and (H).

Isosurfaces in (C)–(H) were rendered at a higher threshold (2σ) to reveal more details.

and edge-to-edge distances (555 Å). Demarcation of the molecular boundaries between the P8 multimers gave detailed insight into the ϕ6 NC shell architecture (Figures 4A and 4B). The NC shell has two types of holes at positions denoted with Roman numerals (Figure 4A). There are 60 type II holes and 60 type III holes, based on nomenclature established earlier (Butcher et al., 1997). P8 is assembled into the particle as a trimer, consistent with dynamic light scattering results (Poranen et al., 2001). A total of 200 copies of the P8 trimers are located around the holes (diameter 30 Å) at the quasi 6-fold positions, following the T = 13 lattice organization (Figures 4A and 4B). A T = 13 lattice can exist in two enantiomers, laevo and dextro. A tilt experiment (Belnap et al., 1997) determined the handedness of the reconstruction and revealed the hand of the P8 layer to be laevo. The hand was consistently assigned in 92 of 96 cases, compared to 46 of 47 cases in the HK97 control (T = 7 laevo), which provided the absolute hand.

In the ϕ6 T = 13 shell, there are four classes of tightly interdigitating P8 trimers (Q, R, S, and T) that are not related by icosahedral symmetry (Figures 4A and 4B). Class Q trimers are closest to the icosahedral 5-fold axes of symmetry, class S trimers are adjacent to the 2-fold axes, class T trimers are at the 3-fold axes, and class R trimers are between the others. The P8 layer is interrupted at the icosahedral 5-fold axes by a disc of the hexameric P4 packaging protein (see below). Thus, 10 P8 monomers, not 13 (as would be expected for a T = 13 lattice), contribute to one asymmetric unit.

We then used 3D density alignment to position the four segmented trimers to a common reference for comparison (Figure 4C). Parts of the class Q trimers closest to the P4 hexamer (see below) are more disordered than in the others (circled in Figures 4C and 5A). S, R, and T trimers are similar to each other, and they could thus be averaged together (Huiskonen et al., 2004) to increase the signal for a detailed analysis (Figures 4D–4F). P8 is a relatively small protein (15.9 kDa). Hence, it is not surprising that the trimer is rather flat (diameter of ~75 Å, height of ~25 Å) to cover the surface of the PC. The volume of this roughly cylindrical shape (~110,000 Å^3) matches the volume reported previously (92,000 Å^3) based on hydrodynamic radius (28 ± 2 Å) (Poranen et al., 2001), supporting our P8 density assignment. Raman spectroscopic measurements have shown that P8 is mainly α helical (Bamford et al., 1993). Our secondary structure prediction agrees with these measurements (Figure S2; α1–α10; 5–15 residues, median length of 8 residues) (Cuff and Barton, 2000). Based on the EM reconstruction, P8 has two domains: a core and a peripheral domain (Figure 4D). We computationally identified (Jiang et al., 2001) eight helices in

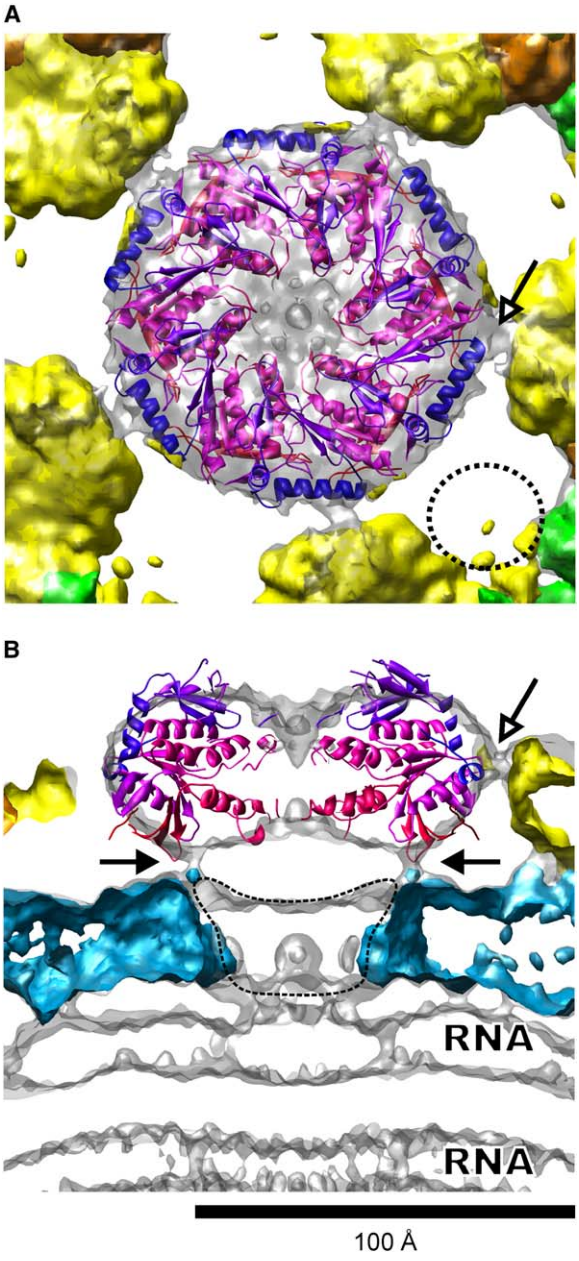

Figure 5. The Vertex Structure

(A and B) The vertex is shown as an isosurface representation from the top in (A) and from the side in (B). The hexameric packaging enzyme P4 X-ray structure from a related virus, ϕ12 (PDB: 1W4C) (Mancini et al., 2004), is shown as a ribbon colored from blue (the N terminus) to red (the C terminus). P1 monomers and P8 trimers are colored as in Figures 2 and 3, respectively. The isosurface was rendered at a low threshold (1σ) to reveal the connections from the P4 density to P1 and P8 (indicated with arrows). One position with a disordered P8 four-helix bundle is circled in (A). Two layers of RNA are labeled, and the unassigned density in the PC shell is indicated with a dashed line in (B). The scale bar represents 100 Å.

each P8 monomer (5–12 residues, median length of 8.5 residues). Four helices (9–12 residues) were found in the core domain, and four short ones (5–8 residues) were found in the peripheral domain (Figures 4D–4F). The helices in the peripheral domain lie approximately normal to the shell (Figure 4F). Their arrangement is similar to a four-helix bundle domain and could correspond to the N terminus of P8, which is predicted (Cuff and Barton, 2000) to contain four consecutive α helices of similar length (Figure S2; α1–α4; 5–9 residues). Both the core and the peripheral four-helix bundle domain interact with the other P8 subunits (Figures 4G and 4H). The core forms tight interactions close to the surface of the shell (Figure 4G). Six helix bundles form a ring around the hexavalent positions in the T = 13 lattice (Figure 4H). The helix bundles are less ordered than the cores (Figure 1B).

The Hexameric Packaging Protein P4 Occupies the Nucleocapsid Vertices and Interacts with P1 and P8

At the 5-fold vertices, a hexamer of P4 protein with 6-fold symmetry is present (de Haas et al., 1999; Mancini et al., 2004). Due to this symmetry mismatch, the P4 hexamer density is incorrectly averaged in the reconstruction process and appears as a disordered disc (Figure 1B, asterisk). The X-ray structure of P4 from a related Cystovirus (ϕ12) is available (Mancini et al., 2004). In addition, the side of P4 that binds to the particle has been determined (Lísal et al., 2006). Thus, we superposed this X-ray structure onto the NC density map in the known orientation (Figure 5). The overall dimensions of the ϕ6 P4 density (diameter of ~105 Å, height of ~60 Å) agree well with the X-ray structure. The diameter is also consistent with that measured from electron micrographs of negatively stained ϕ6 P4 protein (120 Å) (Juuti et al., 1998).

Due to the inappropriate averaging, the rotational fit of the P4 X-ray structure was ambiguous. Despite this, the reconstruction revealed two sites of interaction between the hexamer and its neighboring proteins, P1 and P8 (Figures 5A and 5B, arrows). First, the P4 hexamer density is in very close proximity to the P8 trimers (class Q), and a bridging density was resolved (Figures 5A and 5B, empty arrows). Although the reconstruction reveals the height at which the interactions between P4 and P8 occur, the exact interacting residues remain unknown. The class Q P8 trimers showed disorder (circled in Figures 4C and 5A), a fact that suggests flexibility in the observed interaction between P4 and P8. Second, as expected, the P4 hexamer density also touches the underlaying P1 shell (Figure 5B, filled arrows). One connecting density protrudes upward from each class A P1 monomer toward the adjacent P4 hexamer. These densities are at the same radius as the C-terminal loops pointing downward in the P4 X-ray structure.

Discussion

The ϕ6 NC structure revealed structural similarities to the members of the *Reoviridae* family in the two protein layers and in the RNA genome. In all of these viruses, there is a protein organized on a T = 13 lattice. In ϕ6 and in some members of the *Reoviridae*, such as an orthoreovirus (Dryden et al., 1993; Metcalf et al., 1991) and an aquareovirus (Shaw et al., 1996), the lattice is only partially covered with that protein. A different protein forms turret-like structures at the icosahedral vertices. In orthoreovirus, the turrets are formed by the pentameric RNA-capping protein λ (Reinisch et al., 2000). In aquareovirus, protein VP1 forms the morphologically

equivalent turrets (Nason et al., 2000). In ϕ6, hexameric packaging protein P4 occupies these positions. In bluetongue virus (BTV) and rotavirus, the $T = 13$ shell is complete, and class P trimers occupy the vertices (Grimes et al., 1998; Prasad et al., 1996). The observed structural similarities suggest relatedness between ϕ6 and eukaryotic dsRNA viruses.

The inner protein layer in ϕ6 and in the members of the *Reoviridae* family exhibit the same $T = 1$ architecture, with 60 asymmetric dimers of an α-helical capsid protein. The computational identification of putative helices in ϕ6 P1 protein density agreed well with the secondary structure prediction. In ϕ6, the two types of P1 monomers, A and B, create a dodecahedral organization. Five class A monomers encircle the 5-fold axes, and class B monomers interact at the 2-fold and 3-fold axes. However, L-A and members of the *Reoviridae* family, such as BTV and reovirus, do not exhibit a similar dodecahedral organization. Type A and B monomers interdigitate and encircle the 5-fold axes, type A monomers interact at the 2-fold axes, and type B monomers interact at the 3-fold axes (Grimes et al., 1998; Naitow et al., 2002; Reinisch et al., 2000).

The interior volumes of BTV and ϕ6 are similar, but the BTV genome is larger (19.2 kbp) than that of ϕ6 (13.4 kbp). How does the genome organization reflect this difference? The measured interior volume of the expanded ϕ6 particle (42.4×10^6 Å^3) corresponds to a mean packaging density of ~350 mg/ml for dsRNA, in contrast to ~410 mg/ml in BTV (Gouet et al., 1999). Both BTV and ϕ6 show ordered dsRNA organized as concentric layers. The genome of BTV is in the liquid crystal state and is organized on a hexagonal lattice, with 30 Å interhelix spacing (Gouet et al., 1999). This spacing corresponds to a 26 Å spacing between the layers. The wider spacing between the layers observed in ϕ6 (31 Å) and larger calculated average interhelix spacing (36 Å) is consistent with the estimated lower density of the genome. Assuming that dsRNA behaves similarly to dsDNA, the genome of ϕ6 is in the cholesteric phase (density and interhelix spacing for dsDNA: 160–380 mg/ml and 32–49 Å, respectively), not in the liquid crystal phase (Livolant and Leforestier, 1996). Energetically, in ϕ6, it seems more favorable to have less densely organized RNA filling the entire interior volume (which in turn requires higher RNA curvature) than more densely organized RNA occupying only the larger radii (which in turn would lead to stronger repulsion).

Some of the most intriguing questions to address in the ϕ6 system concern the control of the early stages of assembly. To address how the PC recognizes and packages the three genomic segments, a packaging model has been proposed in which a conformational change occurs in the PC after each segment has been packaged (Mindich, 2004; Qiao et al., 1997). We have previously shown that the dsRNA-containing PC particle isolated from the virion is an expanded form of the naive PC (Butcher et al., 1997). In addition, crosslinking studies have shown that the RNA segments bind most intensively to protein P1 (Qiao et al., 2003). Our segmentation of P1 density, and its modeling into the naive PC, allows us to predict the movement of P1 during the expansion and suggest a mechanism for the RNA packaging specificity. In the expansion model, we see large-scale movement of P1 monomers behaving as rigid bodies (Figure 3; Movie S1). Three observations from the model are relevant to RNA packaging specificity: First, some areas on the class A P1 monomers are fully covered in the naive form. Second, the intermonomer angles (A-A, A-B, B-B) change in the expansion from angled to nearly parallel. Third, the spatial relationship between P4 and P1 varies significantly in the naive and expanded forms (Figure 3B). Consequently, RNA binding sites on P1 could be buried in one capsid expansion state and exposed in another. Furthermore, we suggest that the RNA packaging sites are generated at the quaternary structure level of two or more P1 monomers, not at the tertiary structure level of the individual monomers. This restricts the number of possible binding sites greatly and would allow the RNA to bind specifically proximal to the P4 hexamer. In addition, the binding of RNA to more than one P1 molecule would prevent premature aggregation of the RNA and protein components during assembly. To summarize, we expect that the P1 shell plays a major functional role in recognizing the *pac* sequences on the viral RNA segments. This would align the RNA segments in an orientation promoting packaging by the P4 packaging NTPase. As the PC is a metastable structure, the NTP hydrolysis driving packaging should be sufficient to provide energy for the expansion as well.

The question of how the PC controls the number of packaged segments remains. In our model, at the beginning of packaging, the number of potential s segment *pac* sequence binding sites would be at least 12, yet only 1 s segment is packaged. We propose that the s segment binds in the cup around the 5-fold axis; then, the P4 hexamer ring opens (Lísal et al., 2005), binds close to the 5′ end of the RNA, closes, and starts to package the segment. The packaging is dependent on ATP hydrolysis. Conformational changes in the hexamer subunits propagate sequentially in the hexamer ring and lead to translocation of RNA into the PC (Mancini et al., 2004). This causes a rapid cooperative expansion of the capsid, creating the m binding sites. The cycle would be repeated with packaging of m and l. Once the 3′ end of l has been packaged, the polymerase starts the RNA replication reaction. It has also been proposed that only a single vertex is active in packaging (Pirttimaa et al., 2002). Together with the discussed conformational changes, this would explain the packaging of one copy of each segment.

The ϕ6 packaging and expansion model serves as a paradigm for all dsRNA viruses with segmented genomes. The basic architectures of the $T = 1$ and $T = 13$ layers of ϕ6 are similar to those of other dsRNA viruses, such as the members of the *Reoviridae* family. However, differences also exist. First, the $T = 1$ shell of ϕ6 has a dodecahedral organization. If an unexpanded state exists for the capsids of the members of the *Reoviridae* family, which do not have a similar dodecahedral organization, the inner capsid protein monomers may have to be bent. Second, the packaging enzyme does not seem to be a structural component in the members of the *Reoviridae* family. Analysis of the procapsid structures in eukaryotic dsRNA viruses should reveal whether this proposed model is applicable, or whether they exhibit a completely different packaging strategy.

Experimental Procedures

Isolation and Purification of Virions and NC

Wild-type ϕ6 was propagated in *Pseudomonas syringae* pv *phaseolicola* HB10Y (Vidaver et al., 1973) as described previously (Bamford et al., 1995). To remove the spike protein, P3, purified virions were treated with 4 mM butylated hydroxytoluene (BHT). The envelope of the BHT-treated particles was then solubilized with Triton X-114, releasing NCs as described previously (Bamford et al., 1995).

Electron Microscopy

Vitrified specimens from a 3 μl aliquot of the sample were prepared on holey carbon film (Quantifoil) as described previously (Adrian et al., 1984). The vitrified sample was then observed by using a GATAN 626 or an Oxford CT3500 cryoholder, in an FEI Tecnai F20 field emission gun transmission electron microscope, at −180ºC. Images were taken at a nominal magnification of 50,000× under low-dose conditions. Several different defocus settings were used in order to fill the nodes of the contrast transfer function (CTF) later during the reconstruction (Table 1). Electron micrographs were recorded on Kodak SO163 film and were developed in full-strength D19 for 12 min.

Image Processing and 3D Reconstruction

Micrographs free of astigmatism and drift were scanned at a 7 μm step size on a Zeiss Photoscan TD scanner, resulting in a nominal sampling of 1.4 Å pixel^{-1}. The CTF was estimated from the rotationally averaged power spectrum, obtained by patch averaging of the scanned micrograph by using CTFFIND3 (Mindell and Grigorieff, 2003). Particles were selected automatically by using ETHAN and windowed by using EMAN (Kivioja et al., 2000; Ludtke et al., 1999). These images were normalized for icosahedral reconstruction (Baker and Cheng, 1996; Crowther, 1971; Fuller et al., 1996). Bsoft (Heymann, 2001) was used in further image-processing steps, if not stated otherwise.

The published 3D reconstruction of the NC (Butcher et al., 1997) was used in a model-based parallel approach to determine the orientations and origins of the NC images (Baker and Cheng, 1996; Fuller et al., 1996; Ji et al., 2003). Reconstructions were calculated in Cartesian coordinates (P3DR) (Ji et al., 2003; Marinescu et al., 2001) where a Wiener filter CTF correction was applied. The effective resolution of the models was based on the criterion of the FSC (Harauz and van Heel, 1986) being greater than 0.5 between two independent reconstructions. Reconstruction statistics are listed in Table 1.

The inner volumes of the empty NC reconstruction and a published reconstruction of the unexpanded PC (de Haas et al., 1999) were defined in EMAN (Ludtke et al., 1999). Isosurface representations were created by using the UCSF Chimera (http://www.cgl.ucsf.edu/chimera) (Huang et al., 1996). OpenDX (www.opendx.org) module MAKROVIS was implemented to create masks of different shapes and to analyze disorder in the reconstructions (Figure 1B). For this, isosurface rendering of a given voxel was colored as a function of the maximum density difference between the voxel and its neighbors.

To segment the P1 monomers, an initial mask was created to approximately cover the center of mass of both monomers. These masks were then interactively extended and refined to cover the features shared by both of the monomers, avoiding overlaps between the masks. The segmented P1 monomers were modeled manually into the procapsid reconstruction (de Haas et al., 1999) in UCSF Chimera (Huang et al., 1996). First, the hand of the procapsid reconstruction was inverted to match the determined hand of the NC reconstruction. In addition, a magnification scaling factor of 1.06 was applied to minimize their size difference.

To define the molecular boundaries in the P8 shell, trimer T was first segmented from the rest of the density in EMAN (Ludtke et al., 1999). A dummy-atom model was created from the segmented trimer and fitted into the reconstruction by using CoLoRes (Chacon and Wriggers, 2002) to determine the rotations and translations between all four of the trimers. A binary mask created from trimer T was then used to segment the other trimers. To generate a core difference map, trimers R, S, and T were first averaged together by using the predefined rotations and translations. The averaged trimer was then subtracted from the NC reconstruction at all four trimer positions.

Secondary Structure Analysis

The secondary structure for P1 was predicted by using Jpred (Cuff and Barton, 2000). First, the available P1 sequences (from ϕ6, ϕ8, ϕ12, and ϕ13) were aligned by using T-coffee multiple sequence alignment (Notredame et al., 2000). While the ϕ12 sequence was discarded based on its dissimilarity to ϕ6, the others were used in the prediction. For P8, a similar analysis was performed on the available sequences (from ϕ6, ϕ7, ϕ12, and ϕ13). ϕ6 and ϕ13 P8 sequences provided an informative alignment; the ϕ12 sequence, which was too dissimilar, and ϕ7, which was almost identical to ϕ6, were discarded. The program helixhunter (Jiang et al., 2001) was used to identify putative α helices in the density maps. If a helix was assigned to only one P1 monomer, it was modeled into the corresponding density in UCSF Chimera.

Supplemental Data

Supplemental Data include the sequence alignments and secondary structure predictions for P1 and P8, as well as a movie illustrating the expansion of the PC, and are available at http://www.structure.org/cgi/content/full/14/6/1039/DC1/.

Acknowledgments

The authors gratefully acknowledge the contributions of B. Koli and P. Laurinmäki for technical support and D. Belnap, B. Heymann, and Y. Ji for software and helpful discussions. The MAKROVIS module was implemented by J. Haapasalo, N. Haiminen, M. Huovinen, J. Kervinen, and J. Saukkonen. This work was funded by the National Graduate School in Informational and Structural Biology (J.T.H.), the Academy of Finland Centre of Excellence Programme (2006–2011) (1213467, D.H.B. and S.J.B.), an Academy of Finland Research Fellowship (1208661, S.J.B.), and the European Union (BIO4-CT97-2364, D.H.B. and S.D.F). S.D.F. is a Wellcome Trust Principal Research Fellow.

Received: February 1, 2006
Revised: March 29, 2006
Accepted: March 29, 2006
Published: June 13, 2006

References

Adrian, M., Dubochet, J., Lepault, J., and McDowall, A.W. (1984). Cryo-electron microscopy of viruses. Nature *308*, 32–36.

Baker, T.S., and Cheng, R.H. (1996). A model-based approach for determining orientations of biological macromolecules imaged by cryo-electron microscopy. J. Struct. Biol. *116*, 120–130.

Bamford, D.H., Romantschuk, M., and Somerharju, P.J. (1987). Membrane fusion in prokaryotes: bacteriophage ϕ6 membrane fuses with the *Pseudomonas syringae* outer membrane. EMBO J. *6*, 1467–1473.

Bamford, D.H., Ojala, P.M., Frilander, M., Walin, L., and Bamford, J.K.H. (1995). Isolation, purification and function of assembly intermediates and subviral particles of bacteriophages PRD1 and ϕ6. In Microbial Gene Techniques, K.W. Adolph, ed. (San Diego: Academic Press), pp. 455–474.

Bamford, J.K., Bamford, D.H., Li, T., and Thomas, G.J., Jr. (1993). Structural studies of the enveloped dsRNA bacteriophage ϕ6 of *Pseudomonas syringae* by Raman spectroscopy. II. Nucleocapsid structure and thermostability of the virion, nucleocapsid and polymerase complex. J. Mol. Biol. *230*, 473–482.

Belnap, D.M., Olson, N.H., and Baker, T.S. (1997). A method for establishing the handedness of biological macromolecules. J. Struct. Biol. *120*, 44–51.

Butcher, S.J., Dokland, T., Ojala, P.M., Bamford, D.H., and Fuller, S.D. (1997). Intermediates in the assembly pathway of the double-stranded RNA virus ϕ6. EMBO J. *16*, 4477–4487.

Butcher, S.J., Grimes, J.M., Makeyev, E.V., Bamford, D.H., and Stuart, D.I. (2001). A mechanism for initiating RNA-dependent RNA polymerization. Nature *410*, 235–240.

Caspar, D.L.D., and Klug, A. (1962). Physical principles in the construction of regular viruses. Cold Spring Harb. Symp. Quant. Biol. *27*, 1–24.

Chacon, P., and Wriggers, W. (2002). Multi-resolution contour-based fitting of macromolecular structures. J. Mol. Biol. *317*, 375–384.

Crowther, R.A. (1971). Procedures for three-dimensional reconstruction of spherical viruses by Fourier synthesis from electron micrographs. Philos. Trans. R. Soc. Lond. B Biol. Sci. *261*, 221–230.

Cuff, J.A., and Barton, G.J. (2000). Application of multiple sequence alignment profiles to improve protein secondary structure prediction. Proteins *40*, 502–511.

Day, L.A., and Mindich, L. (1980). The molecular weight of bacteriophage ϕ6 and its nucleocapsid. Virology *103*, 376–385.

de Haas, F., Paatero, A.O., Mindich, L., Bamford, D.H., and Fuller, S.D. (1999). A symmetry mismatch at the site of RNA packaging in the polymerase complex of dsRNA bacteriophage ϕ6. J. Mol. Biol. *294*, 357–372.

Dryden, K.A., Wang, G., Yeager, M., Nibert, M.L., Coombs, K.M., Furlong, D.B., Fields, B.N., and Baker, T.S. (1993). Early steps in reovirus infection are associated with dramatic changes in supramolecular structure and protein conformation: analysis of virions and subviral particles by cryoelectron microscopy and image reconstruction. J. Cell Biol. *122*, 1023–1041.

Fuller, S.D., Butcher, S.J., Cheng, R.H., and Baker, T.S. (1996). Three-dimensional reconstruction of icosahedral particles—the uncommon line. J. Struct. Biol. *116*, 48–55.

Gottlieb, P., Metzger, S., Romantschuk, M., Carton, J., Strassman, J., Bamford, D.H., Kalkkinen, N., and Mindich, L. (1988). Nucleotide sequence of the middle dsRNA segment of bacteriophage ϕ6: placement of the genes of membrane-associated proteins. Virology *163*, 183–190.

Gouet, P., Diprose, J.M., Grimes, J.M., Malby, R., Burroughs, J.N., Zientara, S., Stuart, D.I., and Mertens, P.P. (1999). The highly ordered double-stranded RNA genome of bluetongue virus revealed by crystallography. Cell *97*, 481–490.

Grimes, J.M., Burroughs, J.N., Gouet, P., Diprose, J.M., Malby, R., Zientara, S., Mertens, P.P., and Stuart, D.I. (1998). The atomic structure of the bluetongue virus core. Nature *395*, 470–478.

Harauz, G., and van Heel, M. (1986). Similarity measures between images. Exact filters for general geometry of 3D reconstructions. Optik *73*, 146–156.

Heymann, J.B. (2001). Bsoft: image and molecular processing in electron microscopy. J. Struct. Biol. *133*, 156–169.

Huang, C.C., Couch, G.S., Pettersen, E.F., and Ferrin, T.E. (1996). Chimera: an extensible molecular modeling application constructed using standard components. Pacific Symposium on Biocomputing *1*, 724.

Huiskonen, J.T., Kivelä, H.M., Bamford, D.H., and Butcher, S.J. (2004). The PM2 virion has a novel organization with an internal membrane and pentameric receptor binding spikes. Nat. Struct. Mol. Biol. *11*, 850–856.

Ikonen, T., Kainov, D.E., Timmins, P., Serimaa, R.E., and Tuma, R. (2003). Locating the minor components of double-stranded RNA bacteriophage ϕ6 by neutron scattering. J. Appl. Crystallogr. *36*, 525–529.

Ji, Y., Marinescu, D.C., Zhang, W., and Baker, T.S. (2003). Orientation refinement of virus structures with unknown symmetry. Paper presented at: Proc. 17th Ann. Int'l. Parallel & Distrib. Process. Symp. (Nice, France, IEEE Press).

Jiang, W., Baker, M.L., Ludtke, S.J., and Chiu, W. (2001). Bridging the information gap: computational tools for intermediate resolution structure interpretation. J. Mol. Biol. *308*, 1033–1044.

Juuti, J.T., and Bamford, D.H. (1995). RNA binding, packaging and polymerase activities of the different incomplete polymerase complex particles of dsRNA bacteriophage ϕ6. J. Mol. Biol. *249*, 545–554.

Juuti, J.T., and Bamford, D.H. (1997). Protein P7 of phage ϕ6 RNA polymerase complex, acquiring of RNA packaging activity by in vitro assembly of the purified protein onto deficient particles. J. Mol. Biol. *266*, 891–900.

Juuti, J.T., Bamford, D.H., Tuma, R., and Thomas, G.J., Jr. (1998). Structure and NTPase activity of the RNA-translocating protein (P4) of bacteriophage ϕ6. J. Mol. Biol. *279*, 347–359.

Kenney, J.M., Hantula, J., Fuller, S.D., Mindich, L., Ojala, P.M., and Bamford, D.H. (1992). Bacteriophage ϕ6 envelope elucidated by chemical cross-linking, immunodetection, and cryoelectron microscopy. Virology *190*, 635–644.

Kivioja, T., Ravantti, J., Verkhovsky, A., Ukkonen, E., and Bamford, D. (2000). Local average intensity-based method for identifying spherical particles in electron micrographs. J. Struct. Biol. *131*, 126–134.

Lísal, J., Lam, T.T., Kainov, D.E., Emmett, M.R., Marshall, A.G., and Tuma, R. (2005). Functional visualization of viral molecular motor by hydrogen-deuterium exchange reveals transient states. Nat. Struct. Mol. Biol. *12*, 460–466.

Lísal, J., Kainov, D.E., Lam, T.T., Emmett, M.R., Wei, H., Gottleib, P., Marshall, A.G., and Tuma, R. (2006). Interaction of packaging motor with the polymerase complex of dsRNA bacteriophage. Virology 10.1016/j.virol.2006.03.025.

Livolant, F., and Leforestier, A. (1996). Condensed phases of DNA: structures and phase transitions. Prog. Polym. Sci. *21*, 1115–1164.

Ludtke, S.J., Baldwin, P.R., and Chiu, W. (1999). EMAN: semiautomated software for high-resolution single-particle reconstructions. J. Struct. Biol. *128*, 82–97.

Makeyev, E.V., and Bamford, D.H. (2000). Replicase activity of purified recombinant protein P2 of double-stranded RNA bacteriophage ϕ6. EMBO J. *19*, 124–133.

Mancini, E.J., Kainov, D.E., Grimes, J.M., Tuma, R., Bamford, D.H., and Stuart, D.I. (2004). Atomic snapshots of an RNA packaging motor reveal conformational changes linking ATP hydrolysis to RNA translocation. Cell *118*, 743–755.

Marinescu, D.C., Ji, Y., and Lynch, R.E. (2001). Space-time tradeoffs for parallel 3D reconstruction algorithms for atomic virus structure determination. Concurr. Computat.: Pract. Exper. *13*, 1083–1106.

Mertens, P. (2004). The dsRNA viruses. Virus Res. *101*, 3–13.

Metcalf, P., Cyrklaff, M., and Adrian, M. (1991). The three-dimensional structure of reovirus obtained by cryo-electron microscopy. EMBO J. *10*, 3129–3136.

Mindell, J.A., and Grigorieff, N. (2003). Accurate determination of local defocus and specimen tilt in electron microscopy. J. Struct. Biol. *142*, 334–347.

Mindich, L. (2004). Packaging, replication and recombination of the segmented genome of bacteriophage ϕ6 and its relatives. Virus Res. *101*, 83–92.

Naitow, H., Tang, J., Canady, M., Wickner, R.B., and Johnson, J.E. (2002). L-A virus at 3.4 Å resolution reveals particle architecture and mRNA decapping mechanism. Nat. Struct. Biol. *9*, 725–728.

Nakagawa, A., Miyazaki, N., Taka, J., Naitow, H., Ogawa, A., Fujimoto, Z., Mizuno, H., Higashi, T., Watanabe, Y., Omura, T., et al. (2003). The atomic structure of rice dwarf virus reveals the self-assembly mechanism of component proteins. Structure *11*, 1227–1238.

Nason, E.L., Samal, S.K., and Venkataram Prasad, B.V. (2000). Trypsin-induced structural transformation in aquareovirus. J. Virol. *74*, 6546–6555.

Notredame, C., Higgins, D.G., and Heringa, J. (2000). T-Coffee: a novel method for fast and accurate multiple sequence alignment. J. Mol. Biol. *302*, 205–217.

Olkkonen, V.M., Gottlieb, P., Strassman, J., Qiao, X.Y., Bamford, D.H., and Mindich, L. (1990). In vitro assembly of infectious nucleocapsids of bacteriophage ϕ 6: formation of a recombinant double-stranded RNA virus. Proc. Natl. Acad. Sci. USA *87*, 9173–9177.

Pirttimaa, M.J., Paatero, A.O., Frilander, M.J., and Bamford, D.H. (2002). Nonspecific nucleoside triphosphatase P4 of double-stranded RNA bacteriophage ϕ6 is required for single-stranded RNA packaging and transcription. J. Virol. *76*, 10122–10127.

Poranen, M.M., and Tuma, R. (2004). Self-assembly of double-stranded RNA bacteriophages. Virus Res. *101*, 93–100.

Poranen, M.M., Daugelavicius, R., Ojala, P.M., Hess, M.W., and Bamford, D.H. (1999). A novel virus-host cell membrane interaction. Membrane voltage-dependent endocytic-like entry of bacteriophage ϕ6 nucleocapsid. J. Cell Biol. *147*, 671–682.

Poranen, M.M., Paatero, A.O., Tuma, R., and Bamford, D.H. (2001). Self assembly of a viral molecular machine from purified protein and RNA constituents. Mol. Cell *7*, 845–854.

Prasad, B.V., Rothnagel, R., Zeng, C.Q., Jakana, J., Lawton, J.A., Chiu, W., and Estes, M.K. (1996). Visualization of ordered genomic RNA and localization of transcriptional complexes in rotavirus. Nature *382*, 471–473.

Qiao, X., Qiao, J., and Mindich, L. (1997). Stoichiometric packaging of the three genomic segments of double-stranded RNA bacteriophage ϕ6. Proc. Natl. Acad. Sci. USA *94*, 4074–4079.

Qiao, X., Qiao, J., and Mindich, L. (2003). Analysis of specific binding involved in genomic packaging of the double-stranded-RNA bacteriophage ϕ6. J. Bacteriol. *185*, 6409–6414.

Reinisch, K.M., Nibert, M.L., and Harrison, S.C. (2000). Structure of the reovirus core at 3.6 Å resolution. Nature *404*, 960–967.

Romantschuk, M., and Bamford, D.H. (1985). Function of pili in bacteriophage ϕ6 penetration. J. Gen. Virol. *66*, 2461–2469.

Romantschuk, M., Olkkonen, V.M., and Bamford, D.H. (1988). The nucleocapsid of bacteriophage ϕ6 penetrates the host cytoplasmic membrane. EMBO J. *7*, 1821–1829.

Shaw, A.L., Samal, S.K., Subramanian, K., and Prasad, B.V. (1996). The structure of aquareovirus shows how the different geometries of the two layers of the capsid are reconciled to provide symmetrical interactions and stabilization. Structure *4*, 957–967.

Sinclair, J.F., Tzagoloff, A., Levine, D., and Mindich, L. (1975). Proteins of bacteriophage ϕ6. J. Virol. *16*, 685–695.

Stitt, B.L., and Mindich, L. (1983). The structure of bacteriophage ϕ6: protease digestion of ϕ6 virions. Virology *127*, 459–462.

van Etten, J.V., Lane, L., Gonzalez, C., Partridge, J., and Vidaver, A. (1976). Comparative properties of bacteriophage ϕ6 and ϕ6 nucleocapsid. J. Virol. *18*, 652–658.

Vidaver, A.K., Koski, R.K., and Van Etten, J.L. (1973). Bacteriophage ϕ6: a lipid-containing virus of *Pseudomonas phaseolicola*. J. Virol. *11*, 799–805.

Zhang, X., Walker, S.B., Chipman, P.R., Nibert, M.L., and Baker, T.S. (2003). Reovirus polymerase lambda 3 localized by cryo-electron microscopy of virions at a resolution of 7.6 Å. Nat. Struct. Biol. *10*, 1011–1018.

Zhou, Z.H., Zhang, H., Jakana, J., Lu, X.Y., and Zhang, J.Q. (2003). Cytoplasmic polyhedrosis virus structure at 8 Å by electron cryomicroscopy: structural basis of capsid stability and mRNA processing regulation. Structure *11*, 651–663.

Accession Numbers

The reconstructions have been deposited in the Electron Microscopy Data Bank at the European Bioinformatics Institute with the accession codes EMD-1206 (NC) and EMD-1207 (empty NC).